Atmos. Meas. Tech. Discuss., doi:10.5194/amt-2016-74, 2016
Manuscript under review for journal Atmos. Meas. Tech.
Published: 20 April 2016

Atmospheric Measurement Techniques Discussions

Calculating direct normal irradiance from sun photometer measurements.

Juan Carlos Antuña-Marrero[1], Victoria Eugenia Cachorro[2], Frank García[1], René Estevan[1], Boris Barja[1] and Ángel M. de Frutos[2]

[1] Grupo de Óptica Atmosférica de Camagüey, Centro Meteorológico Provincial de Camagüey, INSMET, Cuba

[2] Grupo de Óptica Atmosférica, Universidad de Valladolid, Spain

Correspondence to: Juan Carlos Antuña-Marrero (jcam45@gmail.com)

Abstract:

An alternative method to modeling is proposed for determining direct normal irradiance from sun photometer measurements. Direct normal irradiance is calculated by integration of the sun photometer spectral irradiance measurements. Using pre and post calibration spectral coefficients and the extraterrestrial spectral irradiances at each filter effective wavelength, digital counts are converted into direct spectral irradiances data. Then the trapezoidal integration procedure is applied to calculate the direct normal beam. The error associated to the integration method is estimated between 6% and 2% depending if the infrared filter is for the 1240 nm or 1640 nm respectively. Validation with collocated quasi-simultaneous manually measured and with modeled direct normal irradiance shows encouraging results. Although the results are not categorically conclusive, they evidence the capabilities of the proposed method for deriving direct normal irradiance under clear sky and also for cloudy

Atmos. Meas. Tech. Discuss., doi:10.5194/amt-2016-74, 2016
Manuscript under review for journal Atmos. Meas. Tech.
Published: 20 April 2016

Atmospheric Measurement Techniques Discussions

conditions. Better results are expected for validations with simultaneous automatic direct normal irradiance measurements.

Key Words: solar radiation, sun photometer, AERONET

1 Introduction:

New satellite missions allowed an accurate quantification of the earth global radiation budget. In contrast, the energy flows inside the climate system and at the earth surface is much less known, because satellites have not the capability to measure those flows directly (Wild et al., 2103). Then, up to the present and in the foreseen future, the instruments located at the surface provide the most accurate measurements of the radiation budget at that level. In that sense over the years, surface networks of solar radiation instruments have been organized worldwide. For example the Baseline Surface Radiation Network (BSRN) (Ohmura, et al., 1998) and the Solar Radiation Network (SolRad-Net) (García et al., 2008; http://solrad-net.gsfc.nasa.gov/).

In particular, SolRad-Net conducts high-frequency total solar flux measurements (305 – 2800 nm) in quasi-real time at several of the Aerosol Robotic NETwork (AERONET) sites, to whom it is associated. Global irradiance measurements from SolRad-Net has been used to validate the AERONET estimates of the radiative forcing and forcing efficiency for variable loading conditions and different aerosol types. Results show a good agreement between the AERONET retrievals and ground based measurements of solar fluxes (García et al., 2008). But SolRad-Net lacks direct solar irradiance measurements, considered among the basics measurements by the BSRN (Ohmura et al., 1998).

Atmos. Meas. Tech. Discuss., doi:10.5194/amt-2016-74, 2016
Manuscript under review for journal Atmos. Meas. Tech.
Published: 20 April 2016

45 The use of numerical models to estimate the solar irradiance and in particular the direct
46 normal irradiance (DNI) dates back to the seventies of the XX century (ex. Bird and
47 Hulstrom, 1981). Notable improvements have been reached but still many studies address
48 this issue, ex. Geymard and Ruiz-Arias, (2015) and references cited in this paper.
49 The lack of DNI measurements at AERONET and SolRad-Net sites have been compensated
50 up to the present by DNI modeling (García et al., 2008). We have implemented an alternative
51 method for the DNI determination, consisting in the integration of the spectral direct solar
52 radiation measurements conducted by a sun photometer (Wobrock and Eiden, 1988; García
53 et al., 2014). Because the method relay on spectral DNI measurements it could be either a
54 complement or an alternative to the DNI modeling.
55 In the next section, we describe the datasets used in this study and the methods applied for
56 measuring, integrating and modeling the DNI. Also the radiative transfer code used for
57 modeling and validating the DNI is described. Following a comparison between integrated,
58 modeled and measured DNI values at Camagüey, Cuba, is shown and the results are
59 discussed.
60

61 **2 Materials and Methods:**

62 **2.1 Dataset and calculation of the spectral direct irradiance.**

63 A Cooperation Agreement between the Grupo de Óptica Atmosférica, Universidad de
64 Valladolid, Spain (GOA-UVA) and the Centro Meteorológico Provincial de Camagüey,
65 Instituto de Meteorología, Cuba (CMPC-INSMET) was signed on 2007. GOA-UVA
66 manages the Red Ibérica de Mediciones de Aerosoles (RIMA) that they created in 2004.
67 Product of the cited agreement on October 2008 a sun photometer was installed at CMPC-

Atmos. Meas. Tech. Discuss., doi:10.5194/amt-2016-74, 2016
Manuscript under review for journal Atmos. Meas. Tech.
Published: 20 April 2016

Atmospheric Measurement Techniques Discussions

INSMET, under the Grupo de Óptica Atmosférica de Camagüey (GOAC) supervision and maintenance at 21.422°N and 77.850°W. Measurements continue up to the present, and they have been contributed to RIMA and in addition to AERONET (Antuña et al., 2012).

Six sun photometers operated between 2008 and 2014 at GOAC's experimental site. Two different configurations of the infrared filters have been present; two sun photometers had a 1240 nm filter and the other four had a 1640 nm filter. Table 1 shows the operation periods, the nominal and effective wavelengths of the filters for each instrument and the two infrared filters configurations. The effect of the different configurations on the calculation of the DNIs will be discussed below.

Each sun photometer is pre and post calibrated. The procedure consist in the determination of the calibration coefficients needed to convert the instrument output digital number to a desired output, in our case radiance (W m^{-2} sr μm^{-1}). The calibration may be conducted in a laboratory using an integrating sphere or in the field using the Langley technique or by inter comparison with reference instruments. Calibration coefficients for the sun photometers installed at Camagüey are retrieved by RIMA personnel according to the standard procedures in place by AERONET (Holben at al., 1998).

Extraterrestrial solar spectral irradiances ($I_{o\lambda}$) at the effective wavelength of each filter were integrated using the equation:

$$I_{o\lambda} = I_{cs\lambda} * e_0 \quad (1)$$

$I_{cs\lambda}$ is the extraterrestrial irradiance from the solar spectrum parameterization (Gueymard, 2004) and e_o is the solar eccentricity is defined as the mean Sun-Earth distance (1AU) divided by the actual Sun-Earth distance squared (Kumar and Umanad, 2005) derived according the

Atmos. Meas. Tech. Discuss., doi:10.5194/amt-2016-74, 2016
Manuscript under review for journal Atmos. Meas. Tech.
Published: 20 April 2016

equation:

$$e_0 = 1 + 0.033 * \cos\left(\frac{2\pi nd}{365}\right) \quad (2)$$

nd is the number of order of the day in the year.

For each sun photometer at each effective wavelength, the rates of the $I_{o\lambda}$ value to the pre and post calibration coefficients were integrated. Those are the conversion coefficients for converting the digital counts into spectral direct irradiance values. Then values of the conversion coefficients for all the days between the pre and post calibration dates were derived by linear interpolation for each one of the effective wavelengths. The former set of daily conversion coefficients at each wavelength were used to calculate the spectral direct irradiance for each observation at each effective wavelength, using the average of the sun photometer triplets' measurements.

2.2 Integrated DNI.

Trapezoidal integration method (Whittaker and Robinson, 1967) was used to integrate the spectral sun photometer measurements to obtain the integrated DNI. To cover the region of the spectrum outside the two extreme sun photometer wavelengths two additional integration points were added, one at each side. They were at the wavelengths of 300 and 2600 nm and the associated values of extraterrestrial spectral direct irradiances (Gueymard, 2004) were used in the integration. The integration intervals were defined by 9 effective wavelengths plus the two additional wavelengths added in each side; 300 and 2600 nm.

The constant contribution of 55.2 W m^{-2} was added to the integral integrated using the trapezoid method, to include the regions from 0.5 nm to 300 nm and from 2600 nm to 10000

Atmos. Meas. Tech. Discuss., doi:10.5194/amt-2016-74, 2016
Manuscript under review for journal Atmos. Meas. Tech.
Published: 20 April 2016

Atmospheric Measurement Techniques Discussions

nm. It was calculated integrating the values of each one of the extraterrestrial spectral irradiance from all the available lines in each one of the two intervals (Gueymard, 2004). The spectral intervals of integration were selected according to the spectral position of each neighbor spectral lines.

For characterizing the error associated to the application of the trapezoidal method to the resolution of the sun photometer measured wavelengths, the extraterrestrial spectrum (Gueymard, 2004) was fully integrated obtaining the solar constant. Then the trapezoidal integration method was applied to the extraterrestrial spectrum, but only taking into account the intensity of spectral lines matching the 9 filters effective wavelengths and the two additional selected, 300 and 2600 nm. The two different filters configuration were taken into account, producing two different results. The comparison of the results obtained with the trapezoidal method of integration with the solar constant, considering both infrared filters configurations, shows an overestimation of 6 % and 2 % for 1240 nm and 1640 nm filters, respectively. Figure 1 illustrates the increase of the integration error in 4% in sun photometers with the 1240 nm filter respect to the ones with the 1640 nm filter. The error of the trapezoidal integration method is the area between the continuous and discontinuous lines and the curve representing the extraterrestrial spectrum. This area is higher in the case of the continuous lines connecting the 1020, 1240 and 2600 nm wavelengths than for the discontinuous line connecting 1020, 1640 and 2600 nm.

Only sun photometer measurements from AERONET Version 2 Direct Sun Algorithm (DSA) products were used in the present study to guarantee the cloud free conditions in the line of sight of the instrument and quality-assured observations (Holben et al., 1998; Smirnov et al., 2000).

Atmos. Meas. Tech. Discuss., doi:10.5194/amt-2016-74, 2016
Manuscript under review for journal Atmos. Meas. Tech.
Published: 20 April 2016

Atmospheric Measurement Techniques Discussions

134

135 **2.3 DNI measurements at Camagüey site.**

136 Hourly measured DNI from the Camagüey meteorological station, located less than 100 m
137 from the sun photometer, were selected. The site operates a Yanishevsky actinometrical
138 station with instruments supplied in the 70s and 80s by the Hydrometeorological Service of
139 the former Soviet Union. The Yanishevsky station consists of an actinometer, model M-3; a
140 pyranometer, models M-80-M or M-115-M; a balanzometer model M-10-M and an analogic
141 galvanometer, models GSA-1MA or GSA-1MB (Antuña et al., 2008). Calibrations of all the
142 instruments are conducted periodically by comparison with a master actinometer and a
143 master pyranometer. Trained observers conduct measurements manually, following the
144 standard methodologies and quality control procedures established for this set of instruments
145 (GGO, 1957). In cases of precipitation or variable cloudiness the time for conducting the
146 actinometrical manual measurements may be extended up to minutes 10 minutes to guarantee
147 that the solar flux remains constant during the entire measurement. (GGO, 1957; GOAC,
148 2010). It could produce time inaccuracies in the register of the observation.
149 Once a measurement is conducted and registered in a notebook designed for that purpose, all
150 the measurement information is digitized using the software Actino version 2.0 (Estevan,
151 2010). This software is an update of the early versions used for the data rescue of the entire
152 1981 to 2005 Camagüey's solar radiation dataset (Antuña et al., 2008). The current version
153 is used operationally for quality controlling, processing and storing the measurements.
154 Actino's outputs also feeds in real time the "Servicio de Diagnóstico de Radiación Solar para
155 Cuba", SDRS (http://www.goac.cu/actino/) and the "Servicio de Diagnóstico de Espesor
156 Óptico para Cuba", SDRS (http://www.goac.cu/eoc/), provided by GOAC. The software

Atmos. Meas. Tech. Discuss., doi:10.5194/amt-2016-74, 2016
Manuscript under review for journal Atmos. Meas. Tech.
Published: 20 April 2016

includes a robust quality control of the input data, its processing and the quality control of the outputs (Antuña et al., 2011). Because of the aging process of the Soviet era instruments, the magnitude of the error associated to the broadband actinometers currently operating in Cuba is estimated around 10 %.

2.4 Modelling DNI.

We used the radiative transfer code developed at the Geophysical Fluid Dynamics Laboratory from the National Oceanic and Atmospheric Administration (Ramaswamy and Freidenreich, 1991; Freidenreich and Ramaswamy, 1999). Vertical profiles of the gasses mass mixing ratio are used by the code. It also includes particulate scattering and absorption, Rayleigh scattering, and gaseous absorption by O_2, O_3, CO_2, and H_2O. Single-scattering properties of clouds and aerosols are integrated into the 25 pseudo-monochromatic bands between 0 and 57 600 cm^{-1}, the solar spectrum is divided for the calculations. The δ-Eddington method is used for reflection and transmission calculus for homogeneous layers and the "doubling-adding" technique to obtain the vertical profiles of flux densities and heating rates.

Prescribed tropical temperature and water vapor mixing ratio profiles (McClatchey, 1972) replaced by the ones determined for Camagüey (Barja and Antuña, 2011). Those profiles were derived from the mean aerological soundings conducted from 1981 to 1988 at Camagüey site (Barja and Antuña, 2008). The values of the pressure, temperature and water vapor mixing ratio at the surface for the site were also used together with monthly mean albedo values for Camagüey (Platero et al., 2015). In addition, the sun photometer derived aerosol optical depth (AOD) at 500 nm and the corresponding solar zenith angle, from AERONET Version 2 DSA products, for the original sun photometer coincident

Atmos. Meas. Tech. Discuss., doi:10.5194/amt-2016-74, 2016
Manuscript under review for journal Atmos. Meas. Tech.
Published: 20 April 2016

measurements, were used for DNI modeling (Holben et al., 1998; Dubovic et al., 2000).

2.5 Coincidence criteria and cloud cover classification.

The applied time coincident criteria consisted in selecting measured DNI, conducted in a time window of ± 5 minutes with respect to the integrated DNI. In case that more than one AERONET Version 2 DSA measurement matched the criteria, only the more near in time measurement was selected and the rest discarded. It was selected taking in consideration the methodology applied for the actinometrical manual measurements. They are conducted in the interval of up to 10 minutes in presence of precipitation or variable cloudiness. In the former conditions, precipitation or variable cloudiness, the extension of the measurement time pursues the goal to guarantee that the solar flux remains constant during the entire measurement. (GGO, 1957; GOAC, 2010). Modeled DNI were only determined for the set of AERONET Version 2 DSA measurements selected from the application of the coincidence criteria.

The set of coincident measured, integrated and modeled DNIs was classified according to following four categories of the tenths of sky cloud cover:

- Cloudiness 0 to 10 (All Sky).
- Cloudiness 0 to 1 (Clear Sky)
- Cloudiness 2 to 6 (Partially Cloudy)
- Cloudiness 7 to 10 (Overcast)

The comparison was conducted between measured and integrated DNI, modeled and integrated DNI and modeled and measured DNI. For each one of those pairwise comparisons the four cloud cover categories were applied and the results depicted in the corresponding

Atmos. Meas. Tech. Discuss., doi:10.5194/amt-2016-74, 2016
Manuscript under review for journal Atmos. Meas. Tech.
Published: 20 April 2016

Atmospheric Measurement Techniques Discussions

scatter diagrams. In addition, least squares linear fits were conducted, determining the slope, intercept correlation coefficient (R) and coefficient of determination (R^2).

3 Validating the integrated DNI.

3.1 Integrated DNI vs. measured DNI:

Figure 2 shows the scatter plots of integrated vs. measured DNI for the four sky cloud cover categories. The respective least squares linear fit for each category is shown in red. Only in the clear sky condition, sky cover 0-1, the points are concentrated mainly around the least squares linear fit with a low dispersion. In the rest of the cloud cover categories, a big dispersion is present, but still a high concentration of points may be appreciated around the same region where the points are concentrated in the clear sky case, but in higher amounts.

In the figure 2 in general for most of the sky cloud cover categories the integrated DNI slightly overestimates the measured DNI. Table 2 reports the slopes and intercepts from the linear fits of all the combinations of comparisons between measured, integrated and modeled DNI, grouped according to the four sky cloud cover categories. The intercepts for the four sky cloud cover categories for the integrated vs. measured DNI range between -100 and 25 Wm^{-2}, indicating the magnitudes of the overestimations of the integrated DNI, in the case of the negative values and the opposite for the positive value in the overcast category.

Table 3 contains the R and R^2 values derived from the linear fits of all the combinations of comparisons between measured, integrated and modeled DNI, grouped according to the four sky cloud cover categories. For the clear sky category, the R-value is 0.92, while for the rest three sky cloud cover categories R is in the order of 0.85, causing the R^2 value of 0.84 for clear sky and for the rest three-sky cloud cover categories to drop to the range between 0.72

Atmos. Meas. Tech. Discuss., doi:10.5194/amt-2016-74, 2016
Manuscript under review for journal Atmos. Meas. Tech.
Published: 20 April 2016

and 0.73. A comparison between modeled and measured DNI at six solar radiation stations located between 23.5 °N and 24.6 °N in the United Arab Emirates (UAE), under clear sky, reports R^2 values ranging between 0.83 and 0.86 (Eissa et al., 2015). The R^2 value of 0.92 under clear sky for the measured and integrated DNI is around 10% higher than the results described for the UAE solar radiation stations between measured and modeled DNI. The fact that UAE stations are automatic tropical stations in the same latitudinal band than Camagüey, allows using the described results to show the feasibility of the proposed method.

3.2 Integrated DNI vs. Modeled DNI:

The scatter plots of integrated vs. modeled DNI for the four-sky cloud cover categories are in figure 3. The dispersion seen in figure 2 decreased and also the magnitude of the intercepts, except for the overcast category, whose value in table 2 range between around -60 and 30 Wm^{-2}. These is the same overestimation of the integrated DNI observed with respect to the measured DNI, in the present case with respect to the modeled DNI, also for all the sky cloud cover categories except for the overcast category. Note that the intercept values, are slightly lower in this case. The values of R, in table 3, for the four sky cloud cover categories are above 0.94, reaching for the clear sky category the value of 0.97, a high value. In the same table 3, R^2 range between 0.88 and 0.94, the last value the one corresponding to the clear sky category. The R^2 value of 0.94 for the clear sky category is well over the values reported by Eissa et al., (2015) demonstrating the potential of the proposed method. Also for the other three sky cloud cover categories the values of R^2 are higher than the reported by the study conducted in the UAE.

Atmos. Meas. Tech. Discuss., doi:10.5194/amt-2016-74, 2016
Manuscript under review for journal Atmos. Meas. Tech.
Published: 20 April 2016

Atmospheric Measurement Techniques Discussions

248 The better results achieved in comparing the integrated DNI with the modeled DNI than in
249 the case of the comparison with the measured DNI, could be attributed to the limitations of
250 the measured DNI dataset. The aging of the actinometrical instruments dating from the
251 Soviet era, represented in the estimated 10% magnitude of the error; the inaccuracy in the
252 exact time the measurements are conducted and other potential issues related to manual
253 measurements represent limitations of the dataset. For that reason, a comparison between
254 the modeled DNI and measured DNI follows.
255
256 **3.3 Modeled DNI vs. measured DNI:**
257 Modeled vs. measured DNI scatter plots, on figure 4, shows a lower dispersion than the
258 integrated vs. measured DNI plot on figure 2, but higher than the one in figure 3 for the
259 integrated vs. modeled DNI. The magnitudes of the intercepts range between around 35 and
260 -14 Wm^{-2}, with the only negative value registered for the clear sky category. Values of R
261 and R^2, in table 3, are very similar to the ones for the integrated vs. measured DNI linear fits,
262 but notably lower than the ones for the integrated vs. modeled DNI comparison
263 The results described above are not categorically conclusive mainly for the limitations of the
264 manual DNI measurements available to test the robustness of the proposed method. But they
265 are encouraging. The comparison of the integrated DNI with the modeled DNI may be
266 considered good results in general for the four sky cloud cover categories, but in particular
267 for the clear sky. Results under cloudy conditions show indications that the method could be
268 also valuable under these sky cover conditions. Under cloudy conditions few models has
269 shown good performance; that is a pending issue in modeling solar radiation. Better results

Atmos. Meas. Tech. Discuss., doi:10.5194/amt-2016-74, 2016
Manuscript under review for journal Atmos. Meas. Tech.
Published: 20 April 2016

are expected for the validation of the method in an AERONET site hosting automatic DNI measurements.

4 Conclusions:

The integrated DNI from spectral sun photometer measurements show a reasonable agreement both with manually measured DNI and with modeled DNI using a state of the art radiative transfer code, adjusted for the location both actinometrical and sun photometer measurements are conducted. Under conditions of no clouds in the line of sight of the sun photometer, the correlation and determination coefficients show good results for the comparison between integrated DNI and both measured and modeled DNI when compared to with results achieved at six tropical stations in the same latitude band. The trapezoidal integration method applied, produces an overestimation error of the integrated DNI between 6% and 2% depending if the configuration of the higher wavelength infrared filter is 1240 nm or 1640 nm respectively. This error is in the same order of magnitude than the error associated to the DNI measured by the manual actinometer. The lack of absolute time coincidence of automatic sun photometer measurements and manually measured DNI is an important source of error.

Under cloudy conditions the method show results equivalent to the ones achieved for the six tropical stations at UAE under clear sky conditions. That is promising, because few models has shown good performance under those conditions. The results are not categorically conclusive, but they show clear indications of the feasibility of the proposed method. Better results are expected when automatic measured DNI will be used for the validation.

Atmos. Meas. Tech. Discuss., doi:10.5194/amt-2016-74, 2016
Manuscript under review for journal Atmos. Meas. Tech.
Published: 20 April 2016

Atmospheric Measurement Techniques Discussions

292 At AERONET sites locations, coincident or not with SolRad-Net instruments, it would be
293 expected that the availability of the integrated DNI would contribute to increase the interest
294 of local host institutions for the continuous overseen operation of the sun photometers. They
295 would become more engaged in the operation of the instruments and its maintenance with
296 the aim to generate research quality data and at the same time additional real time solar
297 radiation information applicable to local services and weather forecasts.
298
299

Atmos. Meas. Tech. Discuss., doi:10.5194/amt-2016-74, 2016
Manuscript under review for journal Atmos. Meas. Tech.
Published: 20 April 2016

References:

Antuña, J.C., Fonte, A., Estevan, R., Barja, B., Acea, R., and Antuña, J.C.: Solar Radiation Data Rescue at Camagüey, Cuba. Bull. Amer. Meteor. Soc., 89, 1507–1511, 2008.

Antuña J. C., Hernández, C., Estevan, R., Barja, B., Fonte, A., Hernández, T., Antuña Jr, J. C.: Camagüey's solar radiation rescued dataset: preliminary applications, Opt. PuraApl., 44 (1), 43-48, 2011.

Antuña, J. C., Estevan, R., Barja, B.: Demonstrating the Potential for First-Class Research in Underdeveloped Countries: Research on Stratospheric Aerosols and Cirrus Clouds Optical Properties, and Radiative Effects in Cuba (1988–2010). Bull. Amer. Meteor. Soc., 93, 1017–1027. doi: http://dx.doi.org/10.1175/BAMS-D-11-00149.1, 2012.

Barja, B. and Antuña, J. C., Numerical simulation of cirrus cloud radiative forcing using lidar backscatter data. Preliminary results, Óptica Pura y Aplicada, 41, 89–95, 2008.

Barja B. and J.C. Antuña, The Effect of the Optically Thin Cirrus Clouds on the Solar Radiation in Camagüey, Cuba, Atmos. Chem. Phys., 11, 8625–8635. doi: http://dx.doi.org/10.5194/acp-11-8625-2011, 2011.

Bird R. E., and R. L. Hulstrom, Review, Evaluation and Improvement of Direct Irradiance Models, J. Sol. Energy Eng. 103, 182-192, doi: http://dx.doi.org/10.1115/1.3266239, 1981.

Dubovik, O., Smirnov, A., Holben, B. N., King, M. D., Kaufman, Y. J., Eck, T. F., and Slutsker, I.: Accuracy assessments of aerosol optical properties retrieved from Aerosol

Atmos. Meas. Tech. Discuss., doi:10.5194/amt-2016-74, 2016
Manuscript under review for journal Atmos. Meas. Tech.
Published: 20 April 2016

Robotic Network (AERONET) Sun and sky radiance measurements, J. Geophys. Res., 105, 9791–9806, doi: http://dx.doi.org/10.1029/2000JD900040, 2000.

Eissa, Y., S. Munawwar, A.l Oumbe, P. Blanc, H. Ghedira, L. Wald, H. Bru c, D. Goffe, Validating surface downwelling solar irradiances estimated by the McClear model under cloud-free skies in the United Arab Emirates. Solar Energy, 114, 17-31, http://dx.doi.org/10.1016/j.solener.2015.01.017, 2015.

Estevan, R.: Certificación de depósito legal facultativo de obras protegidas; software: "Actino 2.0"; CENDA 218-2010. (In Spanish), 2010.

García, O. E., Díaz, A. M., Expósito, F. J., Díaz, J. P., Dubovik, O., Dubuisson, P., Roger, J.-C., Eck, T. F., Sinyuk, A., Derimian, Y., Dutton, E. G., Schafer, J. S., Holben, B. N., and García, C. A.: Validation of AERONET estimates of atmospheric solar fluxes and aerosol radiative forcing by ground-based broadband measurements, J. Geophys. Res., 113, D21207, doi: http://dx.doi.org/10.1029/2008JD010211, 2008.

García, F., Antuña-Marrero, J. C., Cachorro, V., Estevan, R., Barja, B. y de Frutos, A.: Cálculo de irradiancia solar directa de banda ancha empleando las observaciones de un fotómetro solar CIMEL CE-318. Informe Científico Técnico, INSMET, La Habana, Cuba, 13 pag. (In Spanish), 2014.

GGO: Manual for the setup and operation of solar radiation instruments. Ed. Guidrometeoizdat, 124 pp. (In Russian), 1957.

Atmos. Meas. Tech. Discuss., doi:10.5194/amt-2016-74, 2016
Manuscript under review for journal Atmos. Meas. Tech.
Published: 20 April 2016

339 GOAC: Manual de Observaciones Actinométricas. Manual de procedimiento para
340 Observadores Actinométricos, Grupo de Óptica Atmosférica de Camagüey, pp. 37
341 (In Spanish), 2010.

342 Gueymard, C.: The sun's total and spectral irradiance for solar energy applications and solar
343 radiation models. Solar Energy, 76, pp. 423–453, doi:10.1016/j.solener.2003.08.039,
344 2004.

345 Gueymard, C. and J. A. Ruiz-Arias, Validation of direct normal irradiance predictions under
346 arid conditions: A review of radiative models and their turbidity-dependent
347 performance. Renew. Sustain. Energy Rev., 45, 379–396.
348 http://dx.doi.org/10.1016/j.rser.2015.01.065

349 Holben, B.N., Eck, T.F., Slutsker, I., Tanré, D., Buis, J., Setzer, A., Vermote, E.F., Reagan,
350 J.A., Kaufman, Y. J., Nakajima, T., Lavenu, F., Jankowiak, I., and Smirnov, A.:
351 "AERONET – A federated instrument network and data archive for aerosol
352 characterization", Remote Sensing of Environment, 66, 1-16, 1998.

353 Kumar, R. and L. Umanad, Estimation of global radiation using clearness index model for
354 sizing photovoltaic system. Renewable Energy 30, 2221–2233, 2005.

355 Ohmura, A., Gilgen, H., Hegner, H., Müller, G., Wild, M., Dutton, E. G., Forgan, B.,
356 Fröhlich, C., Philipona, R., Heimo, A., König-Langlo, G., McArthur, B., Pinker, R.,
357 Whitlock, C. H., and Dehne, K.: Baseline Surface Radiation Network (BSRN/WCRP):
358 New precision radiometry for climate research. Bull. Am. Meteor. Soc., 79, 2115–
359 2136, 1998.

Platero-Morejón, I. Y., R. Estevan-Arredondo and F. García-Parrado, Climatology of Surface Albedo at Camagüey Actinometric Station. Óptica Pura y Aplicada, 48(4), 259-269, doi: http://dx.doi.org/10.7149/OPA.48.4.259, 2015.

Smirnov A., Holben, B.N., Eck, T.F., Dubovik, O., and Slutsker, I.: Cloud screening and quality control algorithms for the AERONET database, Rem. Sens. Env., 73, 337-349, 2000.

Toledano, C., Cachorro, V.E., Vergaz, R., de Frutos, A.M., Sorribas, M., Vilaplana J.M., y De la Morena, B.: Analysis and correction of a fictitious diurnal cycle in the aerosol optical depth: the KCICLO method. Óptica Pura y Aplicada, 37, pp. 49-60, 2004.

Whittaker, E. T. and Robinson, G.: The Trapezoidal and Parabolic Rules, in: The Calculus of Observations: A Treatise on Numerical Mathematics, 4th ed. New York: Dover, pp. 156-158, 1967.

Wild, M., Folini, D., Schär, C., Loeb, N., Dutton, E. G., and König-Langlo, G.: The global energy balance from a surface perspective, Clim. Dynam., 40, 3107–3134, doi: http://dx.doi.org/10.1007/s00382-012-1569-8, 2013.

Wobrock W., and R. Eiden, Direct solar radiation: spectrum and irradiance derived from sun-photometer measurements, Appl. Opt. 27, 2253-2260, doi: http://dx.doi.org/10.1364/AO.27.002253, 1988.

Atmos. Meas. Tech. Discuss., doi:10.5194/amt-2016-74, 2016
Manuscript under review for journal Atmos. Meas. Tech.
Published: 20 April 2016

Atmospheric Measurement Techniques Discussions

Tables:

Table 1: Operational periods of sun photometers at Camagüey, Cuba. Filters nominal and effective wavelengths for each instrument. The two different configurations of the infrared filters could be appreciated.

Instrument Number	Operations Period		Design Wavelengths (nm)									
	Begin	End	1640	1240	1020	935	870	675	500	440	380	340
425	2008/10/07	2009/04/10	--	1246	1020	937	870	675	498	435	380	339
353	2009/06/04	2010/04/23	--	1247	1021	934	871	674	499	438	380	339
419	2010/06/03	2011/06/17	1624	--	1021	939	869	676	502	442	379	339
424	2011/07/21	2012/07/16	1643	--	1016	934	870	673	499	435	380	339
353*	2012/07/23	2013/05/29	1646	--	1020	934	870	673	500	438	380	339
424	2013/09/30	2014/08/02	1643	--	1016	935	870	674	499	436	381	339

Table 2: Slopes and intercepts from the least squares linear fits of the comparisons between measured, integrated and modeled DNI, grouped according to the four sky clouds cover categories.

	integrated vs. measured DNI		integrated vs. modeled DNI		Modeled vs. Measured DNI		
Sky Cloud Cover	**Slope**	**Intercept**	**Slope**	**Intercept**	**Slope**	**Intercept**	**Cases**
All Sky	0.889	-44.7	1.034	-40.7	0.886	32.2	2382
Clear Sky	0.947	-94.1	1.078	-62.7	1.003	-14.0	185
Partially Cloudy	0.871	-53.8	1.034	-49.7	0.892	26.4	1957
Overcast	0.980	25.0	1.073	33.3	0.852	34.8	240

Atmos. Meas. Tech. Discuss., doi:10.5194/amt-2016-74, 2016
Manuscript under review for journal Atmos. Meas. Tech.
Published: 20 April 2016

Atmospheric Measurement Techniques Discussions

388

389 Table 3: Correlation and determination coefficients from the least squares linear fits of the
390 comparisons between measured, integrated and modeled DNI, grouped according to the four
391 sky clouds cover categories.

392

	Integrated vs. Measured DNI		Integrated vs. Modeled DNI		Modeled vs. Measured DNI		393
Sky Cloud Cover	**R**	**R^2**	**R**	**R^2**	**R**	**R^2**	**Cases**
All Sky	0.851	0.725	0.948	0.899	0.849	0.720	2382
Clear Sky	0.918	0.842	0.967	0.935	0.928	0.861	185
Partially Cloudy	0.846	0.716	0.953	0.907	0.846	0.716	1957
Overcast	0.855	0.730	0.940	0.884	0.857	0.734	240

Atmos. Meas. Tech. Discuss., doi:10.5194/amt-2016-74, 2016
Manuscript under review for journal Atmos. Meas. Tech.
Published: 20 April 2016

Atmospheric Measurement Techniques Discussions

394 Figures:
395

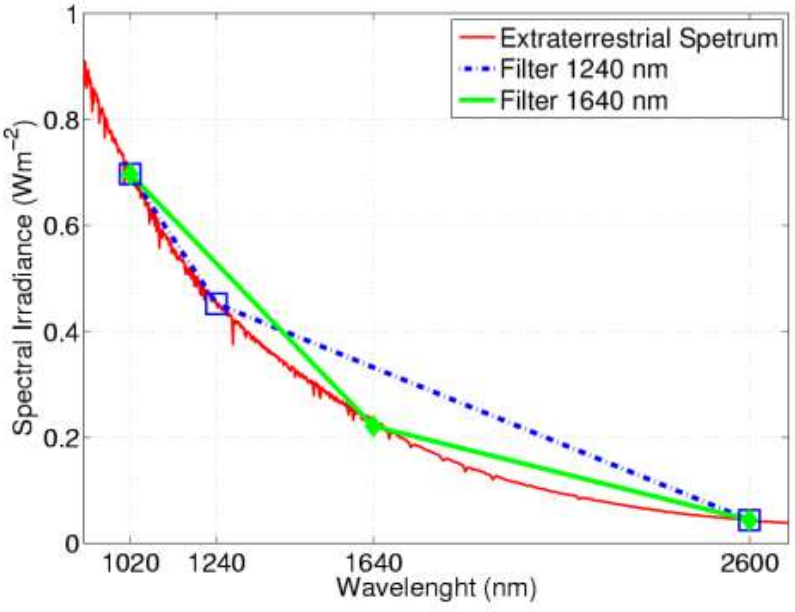

396
397 Figure 1: Illustration of the integration procedure around the filters wavelengths for the
398 region of the extraterrestrial spectrum between 1020 and 2600 nm wavelengths
399 .

Atmos. Meas. Tech. Discuss., doi:10.5194/amt-2016-74, 2016
Manuscript under review for journal Atmos. Meas. Tech.
Published: 20 April 2016

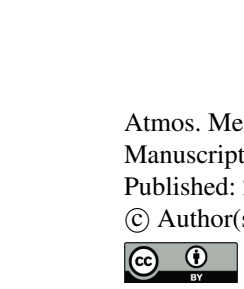

Atmospheric Measurement Techniques Discussions

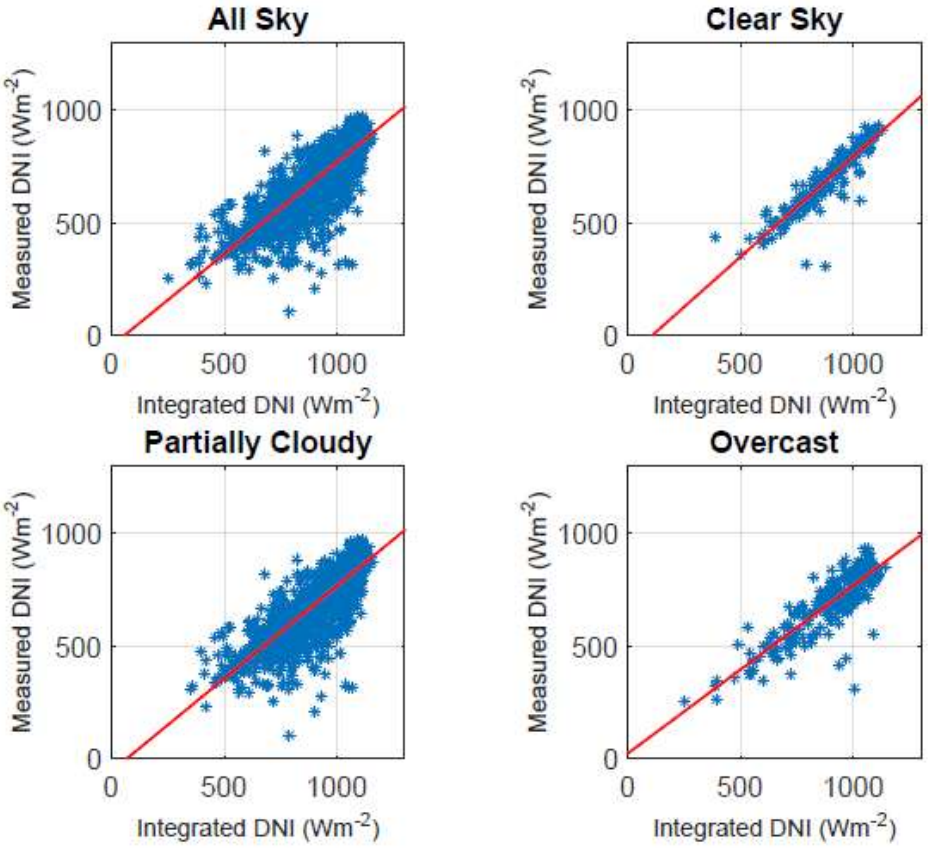

400

401 Figure 2: Scatter plots of the pairs of coincident integrated and measured DNI for the four
402 sky cloud cover categories. The straight-line represents the least squares linear fit.

403

Atmos. Meas. Tech. Discuss., doi:10.5194/amt-2016-74, 2016
Manuscript under review for journal Atmos. Meas. Tech.
Published: 20 April 2016

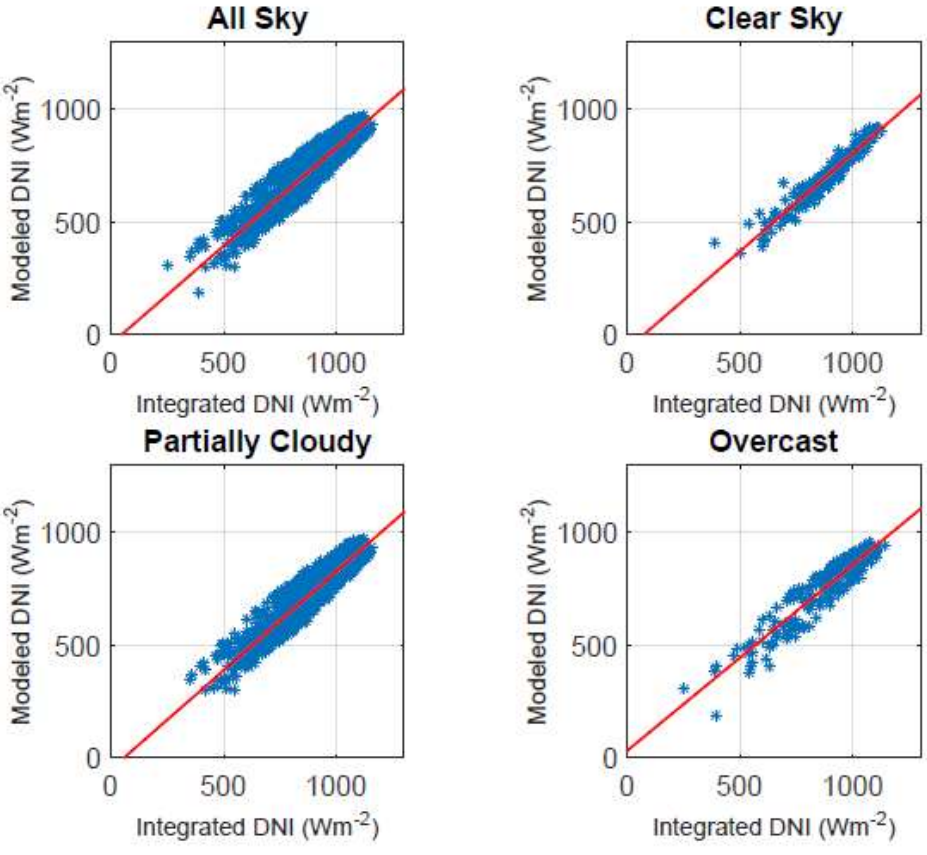

404

405 Figure 3: Idem figure 2, but for the pairs of integrated and modeled DNI.

406

Atmos. Meas. Tech. Discuss., doi:10.5194/amt-2016-74, 2016
Manuscript under review for journal Atmos. Meas. Tech.
Published: 20 April 2016

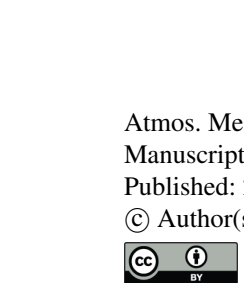

Atmospheric Measurement Techniques Discussions

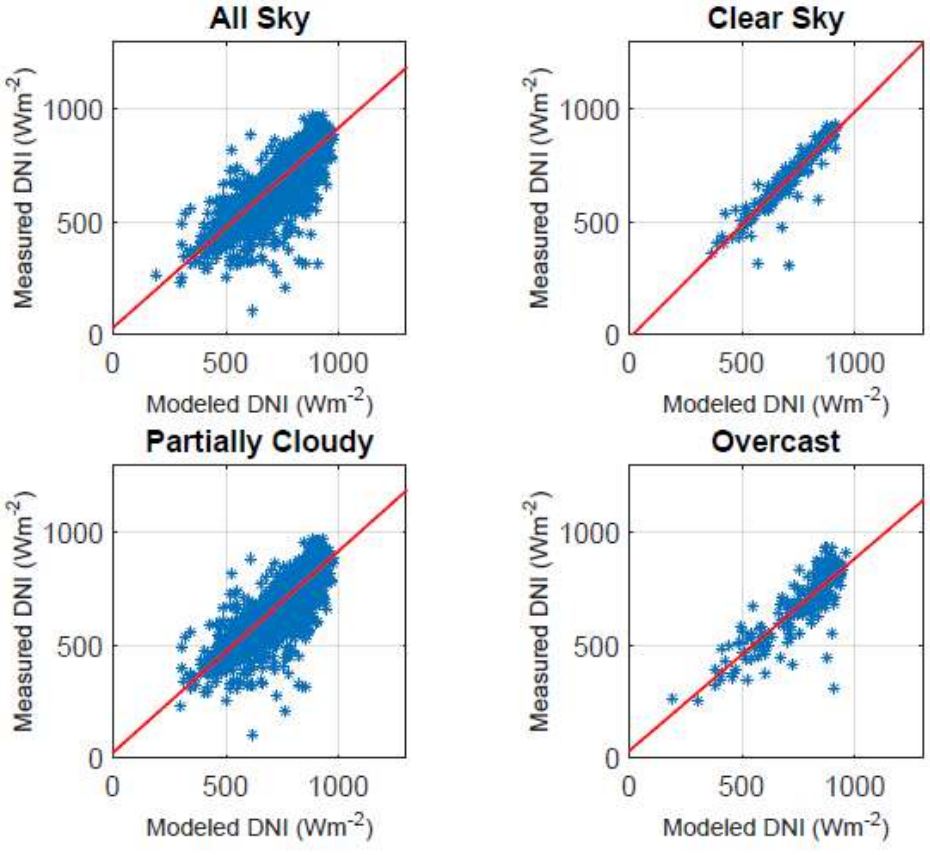

407

408 Figure 4: Idem figure 2, but for the pairs of modeled and measured DNI.